On the Adequacy of the Far-Field Conditions for Pulsed Radiated EM Fields

Lager, Ion E.; Smolders, A.B.

DOI
10.1109/LAWP.2015.2412371

Publication date
2015

Document Version
Accepted author manuscript

Published in
IEEE Antennas and Wireless Propagation Letters

On the Adequacy of the Far-Field Conditions for Pulsed Radiated EM Fields

Ioan E. Lager, *Senior Member, IEEE*, and A. B. Smolders, *Senior Member, IEEE*

***Abstract*—The far-field region's bound is investigated in case of the pulsed electromagnetic field radiation. The value predicted by means of "standard," time-harmonic considerations is compared with that following from the ratio between the maximum value of the time-domain, near- and far-field magnetic field strength constituents. The adequacy of these criteria is analyzed in the case of a loop-to-loop transfer scenario. The obtained results are of relevance for close-range, wireless digital transfers and provide a safety margin for ensuring the adequacy of the "standard" far-field region's limit in ultrawideband links.**

***Index Terms*—Near fields, time-domain analysis, ultrawideband (UWB) antennas.**

I. Introduction

THE ULTRAWIDEBAND (UWB) technology is credited among the most propitious avenues for tackling the ever increasing throughput demand in wireless digital communication. As shown in [1], UWB hinges on pulsed electromagnetic (EM) transfer that yields high data-rates [2] and, possibly, ultralow power consumption [3]–[5]. As with any wireless digital transfer, the pulse detection is cornerstone to implementing robust UWB communications. Due to the very low admissible levels of UWB radiated power [6], the accurate knowledge of the *expected* pulse shape at the receiver side is conditional to implementing effective matched filters for discriminating pulses from noise [7, Section III-B] or for developing low-complexity, direct pulse detection circuitry [8]. Note that transmitted pulse signatures undergo significant spatial transformations, their shape only stabilizing in the *far-field region* [9].

While, theoretically, UWB relies on well established *time-domain* (TD) EM field results [1], the design of such systems is far from trivial. Any such design requires the estimation of the received pulse's shape. This analysis is carried out almost exclusively by means of *time-harmonic* (TH) instruments. Moreover, the radiated EM field is evaluated under the *far-field approximation*, the applicability of which being drawn from the IEEE standard criterion

$$X > 2D^2/\lambda \tag{1}$$

Manuscript received February 13, 2015; revised March 06, 2015; accepted March 09, 2015. Date of publication March 12, 2015; date of current version August 06, 2015.

I. E. Lager is with the Delft University of Technology, 2628 CD Delft, The Netherlands (e-mail: i.e.lager@tudelft.nl).

A. B. Smolders is with the Eindhoven University of Technology, 5600 MB Eindhoven, The Netherlands (e-mail: a.b.smolders@tue.nl)

Color versions of one or more of the figures in this letter are available online at http://ieeexplore.ieee.org.

in which X denotes the distance from the transmitting radiator's reference center, D its diameter and λ the wavelength at the operational frequency f.[1] This condition is derived based on the phase variation on a (conventional) spherical wavefront [11, Section 14.7]—a typical TH consideration. At variance with this, the TD radiated EM field analysis discriminates between near- and far-field regions based on the field dependence on the distance X and on the corresponding time signatures [13, Sections 26.9 and 26.10].

This letter examines the adequacy of pulsed EM *far-field limits* by comparing the values predicted based on TD and "standard" TH arguments in the case of a loop-to-loop, pulsed EM field transfer scenario. Our study is of relevance for close-range, wireless digital communications as considered in [9], [14]. The discussed experiments will evidence that (1) yields a too low bound of the far-field region and, thus, may result in erroneous prediction of the received pulse's shape.

II. Pulsed Radiated EM Field

A. Prerequisites

The EM field radiated by a small, conducting, current-carrying loop $\mathcal{L}$ is studied. The loop is characterized by its reference center $\mathcal{R}$, its circumference C, its diameter D, and its oriented area $\boldsymbol{A}(|\boldsymbol{A}| = A)$, the area's orientation being associated with that of the electric current in the loop. Position with respect to $\mathcal{R}$ is specified by the position vector $\boldsymbol{X}(|\boldsymbol{X}| = X)$. For convenience, in the following we shall only consider circular loops. The time coordinate is denoted as t. Normalized spatial and temporal coordinates are marked with a prime. Propagation occurs in free space, with electric permittivity ε_0, magnetic permeability μ_0 and corresponding wavespeed $c_0 = (\varepsilon_0\mu_0)^{-1/2}$.

B. Excitation

The loop is excited by the electric current $I(t)$

$$I(t) = I_{\mathrm{peak}}\, U(t) \tag{2}$$

in which I_{peak} is the peak current and $U(t)$ is a normalized model pulse shape of unit amplitude. *Causal pulse shapes* are considered in this letter, exclusively. Two features deriving from the pulse's shape are of relevance for our analysis.

1) The (conventional) pulse time width t_{w}, that we take here as the time interval over which the pulse has its fastest temporal variation. This parameter induces a pulse spatial

[1]Other criteria, such as $X \gg D$[11, p. 590] or $X \gg \lambda$[12, p. 141], are also used for characterizing TH, far-field radiation. Since these criteria do not yield explicit far-field limits, we do not account for them in our study.

extent $c_0 t_{\mathrm{w}}$ that, in turn, yields the admissible upper bound of C (see below).

2) The center frequency f_{c} as following from the pulse's spectral diagram $|\hat{U}(\mathrm{j}\omega)|^2$, with the hat denoting the Fourier transform and $\omega = 2\pi f$ the angular frequency. It is used as a reference for FD metrics.

Two model pulses are employed in this letter: a monopulse type pulse for which generating circuitry is readily available, and a theoretical pulse with a flat spectral diagram. Their t_{w} and f_{c} parameters are hereafter discussed.

The time differentiated power exponential pulse ($\mathrm{PE}_{\mathrm{dt}}$*) :* It follows from the normalized power exponential (PE) pulse [15] of pulse rise time [2] $t_{\mathrm{r}} > 0$ and pulse rising power $\nu > 1$ (with $\nu \in \mathbb{N}$ throughout this letter) as

$$\begin{aligned}\mathrm{PE}_{\mathrm{dt}}(t) &= t_{\mathrm{r}} N(\nu) \partial_t \mathrm{PE}(t) \\ &= N(\nu)\left(t'^{\nu-1} - t'^{\nu}\right) \exp\left[-\nu\left(t'-1\right)\right] H(t) \quad (3)\end{aligned}$$

where $t' = t/t_{\mathrm{r}}$, $H(\cdot)$ is the Heaviside unit step function and

$$N(\nu) = \nu^{-1/2}\left(\frac{\nu^{1/2}}{\nu^{1/2}-1}\right)^{\nu-1} \exp(-\nu^{1/2}) \quad (4)$$

ensures a unit amplitude for $\mathrm{PE}_{\mathrm{dt}}$. Its spectral diagram $|\widehat{\mathrm{PE}}_{\mathrm{dt}}(\mathrm{j}\omega)|^2$ (see [15]) peaks at the center frequency

$$f_{\mathrm{c}} = \nu^{1/2}/\left(2\pi t_{\mathrm{r}}\right) \quad (5)$$

and its pulse width is $t_{\mathrm{w}} = t_{\mathrm{r}} N(\nu)$ (see Appendix). Note that [15] has shown the excellent similarity between $\mathrm{PE}_{\mathrm{dt}}$ and the pulse generated by the integrated circuit discussed in [16].

The Power Exponential Modulated, Sinc-Cosine Pulse (PE_{s-c}) : It was introduced in [17] as a causal pulse with a spectral diagram that approximates a rectangular one over a range $[f_{\mathrm{l}}, f_{\mathrm{h}}]$, $0 < f_{\mathrm{l}} < f_{\mathrm{h}}$, with center frequency $f_{\mathrm{c}} = (f_{\mathrm{l}} + f_{\mathrm{h}})/2$ and bandwidth $B = f_{\mathrm{h}} - f_{\mathrm{l}}$. Its expression is

$$\begin{aligned}\mathrm{PE}_{\mathrm{s-c}}(t) &= t'^{\nu} \exp\left[-\nu\left(t'-1\right)\right] \\ &\times \mathrm{sinc}\left[B(t-t_{\mathrm{r}})\right] \cos\left[2\pi f_{\mathrm{c}}(t-t_{\mathrm{r}})\right] H(t) \quad (6)\end{aligned}$$

with $\mathrm{sinc}(x) \overset{\mathrm{def}}{=} \sin(\pi x)/(\pi x)$, for $x \in \mathbb{R}$, t_{r} being the pulse rise time of the modulating PE pulse, and $\nu > 1$. B and t_{r} are interrelated via $t_{\mathrm{r}} = K_{\mathrm{sc}}/B$, with $K_{\mathrm{sc}} \in \mathbb{N},\ K_{\mathrm{sc}} > 2$, while B and f_{c} are interrelated via $B_{\mathrm{rel}} = B/f_{\mathrm{c}}$, with $B_{\mathrm{rel}} \in [0, 2]$ being the relative bandwidth [17]. The pulse width is taken as

$$t_{\mathrm{w}} = (2f_{\mathrm{c}})^{-1} = B_{\mathrm{rel}}(2K_{\mathrm{sc}})^{-1}\, t_{\mathrm{r}} \quad (7)$$

(see Appendix). The pulse's spectral diagram $|\widehat{\mathrm{PE}}_{\mathrm{s-c}}(\mathrm{j}\omega)|^2$ was shown in [17] to approximate very well a rectangular shape and is, practically, symmetric about f_{c}.

C. Radiated Field

The magnetic field strength $\boldsymbol{H}$ generated by $\mathcal{L}$ is given by [13, p. 761], [9]

$$\boldsymbol{H}(\boldsymbol{X}, t) = \boldsymbol{H}^{\mathrm{NF}}(\boldsymbol{X}, t) + \boldsymbol{H}^{\mathrm{IF}}(\boldsymbol{X}, t) + \boldsymbol{H}^{\mathrm{FF}}(\boldsymbol{X}, t) \quad (8)$$

with $\boldsymbol{H}^{\mathrm{NF}}$ denoting the *near-field constituent*

$$\boldsymbol{H}^{\mathrm{NF}}(\boldsymbol{X}, t) = \left[3\left(\boldsymbol{\Xi} \cdot \boldsymbol{A}\right)\boldsymbol{\Xi} - \boldsymbol{A}\right] \frac{I(t - X/c_0)}{4\pi X^3} \quad (9)$$

$\boldsymbol{H}^{\mathrm{IF}}$ the *intermediate-field constituent*

$$\boldsymbol{H}^{\mathrm{IF}}(\boldsymbol{X}, t) = \left[3\left(\boldsymbol{\Xi} \cdot \boldsymbol{A}\right)\boldsymbol{\Xi} - \boldsymbol{A}\right] \frac{\partial_t I(t - X/c_0)}{4\pi c_0 X^2} \quad (10)$$

and $\boldsymbol{H}^{\mathrm{FF}}$ the *far-field constituent*

$$\boldsymbol{H}^{\mathrm{FF}}(\boldsymbol{X}, t) = \left[\left(\boldsymbol{\Xi} \cdot \boldsymbol{A}\right)\boldsymbol{\Xi} - \boldsymbol{A}\right] \frac{\partial_t^2 I(t - X/c_0)}{4\pi c_0^2 X}.$$

Here $\boldsymbol{\Xi} = \boldsymbol{X}/X$ is the unit vector from $\mathcal{R}$ to the observation point. Equations (9)–(11) are derived by assuming that the electric current has negligible spatial variation along $\mathcal{L}$ that, in turn, requires C to be small with respect to the spatial extent of the feeding pulse $c_0 t_{\mathrm{w}}$.

III. Far-Field Conditions for Radiated EM Fields

Equations (9)–(11) yield the following metrics for assessing the field behavior in the three EM field radiation regions:

$$R_{\mathrm{N;F}}(X') = \frac{|\boldsymbol{H}^{\mathrm{NF}}(\boldsymbol{X}, t)|_{\max}}{|\boldsymbol{H}^{\mathrm{FF}}(\boldsymbol{X}, t)|_{\max}} = \frac{|I(t)|_{\max}}{X'^2 t_{\mathrm{w}}^2 |\partial_t^2 I(t)|_{\max}} \quad (12)$$

$$R_{\mathrm{N;I}}(X') = \frac{|\boldsymbol{H}^{\mathrm{NF}}(\boldsymbol{X}, t)|_{\max}}{|\boldsymbol{H}^{\mathrm{IF}}(\boldsymbol{X}, t)|_{\max}} = \frac{|I(t)|_{\max}}{X' t_{\mathrm{w}} |\partial_t I(t)|_{\max}} \quad (13)$$

in which $X' = X/(c_0 t_{\mathrm{w}})$. For the considered pulses, the ratios $|I(t)|_{\max}/[t_{\mathrm{w}}|\partial_t^2 I(t)|_{\max}]$ and $|I(t)|_{\max}/[t_{\mathrm{w}}|\partial_t I(t)|_{\max}]$ are functions of the corresponding pulse parameters.[3] The EM radiation regions are taken as: *far-field region*, for $X' > X'_{\mathrm{F};t}$, with $R_{\mathrm{N;F}}(X'_{\mathrm{F};t}) = \rho_{\mathrm{N;F}}$ and, *intermediate-field region*, for $X' \in (X'_{\mathrm{N};t}, X'_{\mathrm{F};t})$, with $R_{\mathrm{N;I}}(X'_{\mathrm{N};t}) = \rho_{\mathrm{N;I}}$. The parameters $\rho_{\mathrm{N;F}}$ and $\rho_{\mathrm{N;I}}$ must ensure that $\boldsymbol{H}^{\mathrm{NF}}(\boldsymbol{X}, t)$ is dominated in the far- and intermediate-field regions by $\boldsymbol{H}^{\mathrm{FF}}(\boldsymbol{X}, t)$ and $\boldsymbol{H}^{\mathrm{IF}}(\boldsymbol{X}, t)$, respectively, taking $\rho_{\mathrm{N;F}}$ and $\rho_{\mathrm{N;I}}$ as 0.5 being deemed sufficient to this end.

For comparing $X'_{\mathrm{N};t}$ and $X'_{\mathrm{F};t}$ with the limit given by (1), the loop's circumference is expressed as $C = K_\lambda \lambda_{\mathrm{c}}$ with K_λ a scaling factor and λ_{c} the free space wavelength at the center frequency f_{c}. With this choice, (1) becomes

$$X'_{\mathrm{F};f}(K_\lambda, \nu) = \frac{4K_\lambda^2}{\pi\sqrt{\nu}N'(\nu)} \quad (14)$$

for a $\mathrm{PE}_{\mathrm{dt}}$ excitation and

$$X'_{\mathrm{F};f}(K_\lambda, B_{\mathrm{rel}}, K_{\mathrm{sc}}) = \frac{4K_\lambda^2}{\pi^2} \quad (15)$$

for a $\mathrm{PE}_{\mathrm{s-c}}$ excitation. Note that, for impedance matching, K_λ should be close to one. However, this choice results in loop circumferences that are not small with respect to $c_0 t_{\mathrm{w}}$. In our experiments we take $K_\lambda = 0.6$, this offering an acceptable compromise between these conflicting conditions.

IV. Illustrative Experiments

A first experiment concerns the evaluation of $R_{\mathrm{N;F}}(X')$ and $R_{\mathrm{N;I}}(X')$ for $\mathrm{PE}_{\mathrm{dt}}$ excitations with varying pulse rising powers ν. The relevant plots are shown in Fig. 1. The $X'_{\mathrm{F};f}$ values

[2]The rise time t_{r} of the causal, unipolar PE pulse is defined as the time needed for the pulse to reach its amplitude.

[3]These ratios were determined in our experiments numerically, by examining the relevant time signatures over suitable time-windows.

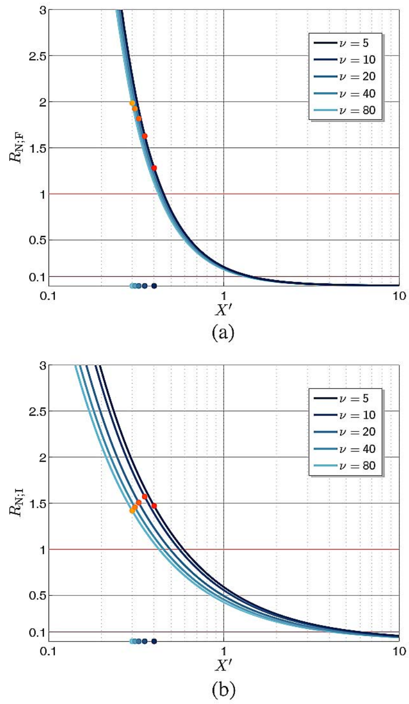

Fig. 1. Constituents ratios dependence on $X' = X/(c_0 t_{\mathrm{w}})$ for $\mathrm{PE}_{\mathrm{dt}}$ pulses with various pulse rising powers ν. (a) $R_{\mathrm{N;F}}(X')$; (b) $R_{\mathrm{N;I}}(X')$. The markers on the ordinates' axis indicate the normalized far-field limit $X'_{\mathrm{F};f}(0.6, \nu)$, their corresponding ratio values being marked by bullets.

TABLE I
$R_{\mathrm{N;F}}(X')$ RATIOS AT $X'_{\mathrm{F};f}(0.6, \nu)$ IN FIG. 1

ν	5	10	20	40	80
$R_{\mathrm{N;F}}[X'_{\mathrm{F};f}(0.6, \nu)]$	1.28	1.63	1.82	1.92	1.98

given by (14) are indicated on the ordinates axes and the corresponding ratios are marked on the relevant plots and given in Table I. The plots show that the near-field constituent is dominant at the standardly predicted far-field region's limit. As expected, the ratios drop rapidly and the far-field constituent becomes dominant at $X' \approx 3X'_{\mathrm{F};f}$.

The first experiment concerned a pulse that is intrinsically wideband. Since in practical situations the transmitted signal is band-limited, a second experiment is carried out by using a $\mathrm{PE}_{\mathrm{s-c}}$ pulse. The $R_{\mathrm{N;F}}(X')$ is plotted in Fig. 2 for relative bandwidths of 100%, 10%, and 1%, respectively. The $X'_{\mathrm{F};f}$ values given by (14) are again indicated on the ordinates axes, with the corresponding ratios being marked on the plots and given in Table II. Fig. 2 demonstrates an accentuated increase of $R_{\mathrm{N;F}}(X')$ as K_{sc} increases,[4] while the influence of B_{rel} on the behavior of $R_{\mathrm{N;F}}(X')$ is limited. We can now infer that a sharp bandpass filtering may result in large near-field constituents for both narrowband and UWB baseband signals. As with the $\mathrm{PE}_{\mathrm{dt}}$ feeding, the far-field constituent becomes dominant at $X' \approx 3X'_{\mathrm{F};f}$.

Our study allows concluding that (12) provides a more adequate basis for estimating the far-field region's bound. As for the value predicted by (1), despite the far-field constituent becoming rapidly dominant, the inadequate limit estimate may

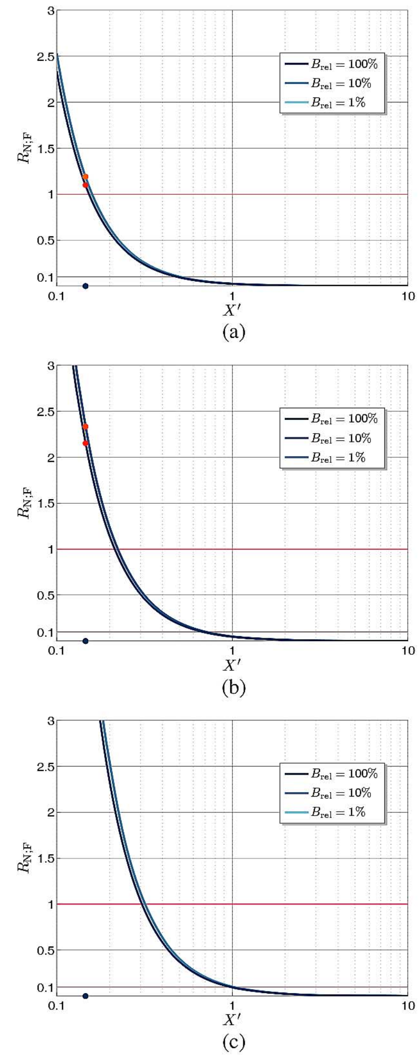

Fig. 2. $R_{\mathrm{N;F}}(X')$ dependence on $X' = X/(c_0 t_{\mathrm{w}})$ for $\mathrm{PE}_{\mathrm{s-c}}$ pulses with various pulse relative bandwidths B_{rel} and K_{sc} values. (a) $K_{\mathrm{sc}} = 5$; (b) $K_{\mathrm{sc}} = 7$; (c) $K_{\mathrm{sc}} = 10$. The markers on the ordinates' axis indicate the normalized far-field limit $X'_{\mathrm{F};f}(0.6, B_{\mathrm{rel}}, K_{\mathrm{sc}})$, their corresponding ratio values being marked by bullets.

TABLE II
$R_{\mathrm{N;F}}(X')$ RATIOS AT $X'_{\mathrm{F};f}(0.6, B_{\mathrm{rel}}, K_{\mathrm{sc}})$ IN FIG. 2

K_{sc}	5	7	10
$R_{\mathrm{N;F}}[X'_{\mathrm{F};f}(0.6, 100\%, K_{\mathrm{sc}})]$	1.10	2.15	4.39
$R_{\mathrm{N;F}}[X'_{\mathrm{F};f}(0.6, 10\%, K_{\mathrm{sc}})]$	1.19	2.33	4.76

be detrimental in critical situations, such as those concerning close-range, UWB communications of the type required by, for example, the energetically self-sustainable wireless networks at the core of Internet of Things scenarios [3], [4].

V. CONCLUSION

The pulsed EM field, far-field region's limit was evaluated based on the "standard," time-harmonic condition and the ratio between the maximum value of the near- and far-field magnetic field strength constituents. Illustrative experiments have

[4]In [17], it was shown that the increase in K_{sc} induces an increasingly sharper spectral diagram slope.

shown that the near-field constituent can be the dominant one at the "standard" limit, this categorically influencing the received pulse's shape. In the case of close-range, ultrafast digital transfers, our study recommends discriminating between the near- and far-field regions based on the near- to far-field constituents' ratio. Furthermore, we suggest a safety margin of $\times 3$ for ensuring the adequacy of the "standard" far-field region's limit in the case of pulsed EM field radiation.

The derived results may serve a purpose in the design of the antenna systems for close range, digital communication and in a more adequate estimation of the corresponding received pulses' shapes.

Appendix
Derivation of the Employed Pulse Widths

1) *The PE_{dt} pulse* In line with [15], the pulse time width t_{w} is obtained as

$$\begin{aligned} t_{\mathrm{w}} &= \int_0^{t_{\mathrm{r}}} \mathrm{PE}_{\mathrm{dt}}(t)\, t = t_{\mathrm{r}} \int_0^{t_{\mathrm{r}}} N(\nu)\partial_t \mathrm{PE}(t)\, t \\ &= t_{\mathrm{r}} N(\nu)\ \mathrm{PE}(t)\big|_{t=0}^{t_{\mathrm{r}}} = t_{\mathrm{r}} N(\nu) \end{aligned} \tag{16}$$

where use was made of $\mathrm{PE}_{\mathrm{dt}}$ having unit amplitude and of the relations $\mathrm{PE}(0) = 0$ and $\mathrm{PE}(t_{\mathrm{r}}) = 1$ (see [15]).

2) *The PE_{s-c} pulse*: For determining the applicable pulse time width t_{w}, (6) is rewritten as

$$\begin{aligned} &\mathrm{PE}_{\mathrm{s-c}}(t) \\ &\quad = t'^{\nu} \exp\left[-\nu\left(t'-1\right)\right] \\ &\qquad \times \mathrm{sinc}\left[K_{\mathrm{sc}}\left(t'-1\right)\right] \cos\left[2\pi K_{\mathrm{sc}}/B_{\mathrm{rel}}\left(t'-1\right)\right] H(t). \end{aligned} \tag{17}$$

This relation induces three characteristic pulse widths:

- $t_{\mathrm{w;PE}}$, corresponding to the PE. By using [15, Eq. (45)], $t_{\mathrm{w;PE}} \in (1.75 t_{\mathrm{r}}, 0.33 t_{\mathrm{r}})$ for $\nu < 55$ (this covering all cases of practical relevance).
- $t_{\mathrm{w;sinc}}$, corresponding to the sinc part; in view of the definition of the sinc

$$t_{\mathrm{w;sinc}} = B^{-1} = K_{\mathrm{sc}}^{-1}\, t_{\mathrm{r}}. \tag{18}$$

  It then follows that $t_{\mathrm{w;sinc}} < t_{\mathrm{w;PE}}$ for $K_{\mathrm{sc}} > 3$.
- $t_{\mathrm{w;cos}}$ corresponding to the cosine part; it is taken as

$$t_{\mathrm{w;cos}} = (2 f_{\mathrm{c}})^{-1} = B_{\mathrm{rel}} (2 K_{\mathrm{sc}})^{-1}\, t_{\mathrm{r}}. \tag{19}$$

  In view of $B_{\mathrm{rel}} \leq 2$, it is clear that $t_{\mathrm{w;cos}} \leq t_{\mathrm{w;sinc}}$.

Since t_{w} corresponds to the pulse's fastest temporal variation, we choose $t_{\mathrm{w}} = t_{\mathrm{w;cos}}$, (19) being used in the main text.

Acknowledgment

The authors would like to thank Professor A. T. de Hoop for his constant guidance and instrumental conceptual clarifications.

References

[1] R. J. Fontana, "Recent system applications of short-pulse ultra-wideband (UWB) technology," *IEEE Trans. Microw. Theory Tech.*, vol. 52, no. 9, pp. 2087–2014, Sep. 2004.

[2] F. Zhang, A. Jha, R. Gharpurey, and P. Kinget, "An agile, ultra-wideband pulse radio transceiver with discrete-time wideband-IF," *IEEE J. Solid-State Circuits*, vol. 44, no. 5, pp. 1336–1351, May 2009.

[3] M. Gorlatova *et al.*, "Energy harvesting active networked tags (EnHANTs) for ubiquitous object networking," *IEEE Commun. Mag.*, vol. 17, no. 6, pp. 18–25, Dec. 2010.

[4] M. Gorlatova, "Energy harvesting networked nodes: Measurements, algorithms, and prototyping," Ph.D. dissertation, Grad. School Arts Sci., Columbia University, NY, New York, USA, 2013 [Online]. Available: http://academiccommons.columbia.edu/item/ac:161643

[5] R. Dokania, X. Wang, S. Tallur, C. Dorta-Quinones, and A. Apsel, "An ultralow-power dual-band UWB impulse radio," *IEEE Trans. Circuits Syst. II, Exp. Briefs*, vol. 57, no. 7, pp. 541–545, Jul. 2010.

[6] National Telecommunications, and Information Administration, "Manual of regulations and procedures for federal radio frequency management," Revision of the 2008 ed., May 2011 [Online]. Available: http://www.ntia.doc.gov/files/ntia/publications/manual_5_11.pdf

[7] B. Sklar, *Digital Communications. Fundamentals and Applications*, 2nd ed. Upper Saddle River, NJ, USA: Prentice-Hall, 2001.

[8] C. Chen, M. A. Do, K. S. Yeo, and C. C. Boon, "A low power UWB direct conversion receiver with pulse detectors," in *Proc. ISOCC*, Busan, Korea, Nov. 2009, pp. 17–20.

[9] I. E. Lager and A. T. de Hoop, "Loop-to-loop pulsed electromagnetic field wireless signal transfer," in *Proc. 6th EuCAP*, Prague, Czech Republic, Mar. 2012, pp. 786–790.

[10] *IEEE Standard Definitions of Terms for Antennas*, 145-1993, IEEE Standards Board, New York, NY, USA, Apr. 23, 2013.

[11] S. J. Orfanidis, "Electromagnetic waves and antennas," Accessed Mar. 3, 2015 [Online]. Available: www.ece.rutgers.edu/~orfanidi/ewa

[12] C. A. Balanis, *Antenna Theory: Analysis and Design*, 2nd ed. New York, NY, USA: Wiley, 1997.

[13] A. T. de Hoop, *Handbook of Radiation and Scattering of Waves*. London, U.K.: Academic, 1995, Electronic reproduction (with corrections) 2008, freely downloadable, for private use, from http://www.atdehoop.com.

[14] I. E. Lager, V. Voogt, and B. J. Kooij, "Pulsed EM field, close-range signal transfer in layered configurations–a time-domain analysis," *IEEE Trans. Antennas Propag.*, vol. 62, no. 5, pp. 2642–2651, May 2013.

[15] I. E. Lager, A. T. de Hoop, and T. Kikkawa, "Model pulses for performance prediction of digital microelectronic systems," *IEEE Trans. Compon., Packag., Manuf. Technol.*, vol. 2, no. 11, pp. 1859–1870, Nov. 2012.

[16] F. Zito, D. Pepe, and D. Zito, "UWB CMOS monocycle pulse generator," *IEEE Trans. Circuits Syst. I, Reg. Papers*, vol. 57, no. 10, pp. 2654–2664, Oct. 2010.

[17] I. E. Lager and A. T. de Hoop, "Causal pulses with rectangular spectral content: A tool for TD analysis of UWB antenna performance," *IEEE Antennas Wireless Propag. Lett.*, vol. 12, pp. 1488–1491, 2013.